Chapter 10

Stabilization calculations for highly excited vibrational levels of the $HeBr_2$ van der Waals cluster

Tomás González–Lezana, Marta I. Hernández, Gerardo Delgado–Barrio and Pablo Villarreal

Instituto de Matemáticas y Física Fundamental (C.S.I.C.)
Serrano 123, E-28006-Madrid (SPAIN) [1]

10.1 Introduction

Rare gas-halogen van der Waals (vdW) complexes are suitable systems to study a great variety of energy transfer processes. For these molecules, vibrational predissociation (VP) is the main mechanism after the laser excitation from the ground (X) to an upper electronic state (B): transfer of vibrational energy from the streching motion of the halogen diatomic partner produces the break of the weak vdW bond between the rare gas atom and the diatom. This process can proceed via direct coupling between the initial vibrational state and dissociative continua or through some intermediate (doorway) state. It has been found that this last mechanism of intramolecular vibrational redistribution (IVR) drives the fragmentation of several vdW complexes such as ArI_2[1], $ArCl_2$[2, 3], NeI_2 [4] and $HeBr_2$[5, 6, 7]. For ArI_2[1], large oscillations of VP rate constants with initial I_2 vibrational state, v, were explained by means of a few-state IVR effect. The same interpretation was given [3]

[1]L.A. Montero, L.A. Díaz and R. Bader (eds.), Introduction to Advanced Topics of Computational Chemistry, 285 - 307, 2003,

for highly structured rotational distributions experimentally found [2] in the fragmentation of $ArCl_2$ within the $\Delta v = -2$ regime (where at least two vibrational quanta are transferred to the vdW bond). For NeI_2, a configuration interaction of a few zero-order quasibound levels was attributed as the responsible effect of the erratic dependence of resonance widths with the diatomic vibrational state [4]. Strong dependence of lifetimes and spectral shifts with v, complicated structures in fragmentation cross sections [5, 6] and rotational distributions [7] for high vibrational levels suggest a similar IVR effect for $HeBr_2$. The study of these levels where the $HeBr_2$ dissociation shifts from a direct mechanism to one involving IVR is the aim of this work.

Since its first experimental detection by van der Burgt *et al.*, [8] $HeBr_2$ has been the subject of several experimental [9, 10, 11] as well as theoretical [5, 6, 7, 12, 13] works. Pioneering van der Burgt's laser induced fluorescence study [8] allowed the determination of a preferred T–shaped geometry and also the measurement of VP linewidths and lifetimes. The authors observed a strong dependence of these magnitudes on the Br_2 vibrational excitation, v. A later analysis of product state distributions extracted from unresolved bands [9] allowed to conclude that $HeBr_2$ dissociation is mainly a vibrational to translational, V $\rightarrow$ T, process which involves little excitation of the rotational motion of the diatomic fragment. Jahn *et al.* [10] studied B state vibrational levels $v = 34 - 48$ using the pump–probe technique. This work enabled the determination of B and X vdW binding energies, lifetimes and spectral blueshifts for the levels under study. The latter presented an erratic behavior for high vibrational states as v increases. Closing of the $\Delta v = -1$ channel for VP was found to occur at $v = 44$. This result was later confirmed by three dimensional calculations performed by González-Lezana *et al.* [5]. More data for linewidths and blueshifts have been recently published by Jahn *et al.* [11] for the region $v = 8 - 12$. These low vibrational states were also the subject of wavepacket calculations performed by Krause and Clary[13]. Good agreement with Golden Rule (GR) calculations was achieved for resonance energies and lifetimes. Three dimensional line shape (LS) calculations also gave good agreement with GR results for low Br_2 vibrational levels. Using both (GR and LS) approaches, almost identical half widths and spectral shifts were obtained up to $v = 24$[5]. For higher v's, deviations for the shifts were explained as a consequence of the neglected bound–bound coupling terms within the GR approach, whereas differences between LS and GR half widths were justified in terms of the energy gap law [14].

Special emphasis on the study of high vibrational levels near the closing of the $\Delta v = -1$ dissociation channel has been made in recent works[5, 6, 7, 12]. Stabilization and close–coupling studies were carried out to study in detail the VP dynamics for $v = 45$[6], the first vibrational level for which dissociation through the $\Delta v = -1$ channel is not possible. An IVR process was suggested to explain the dynamics at such vibrational regime. That possibility has also been confirmed in a combined experimental–theoretical study of $HeBr_2$ product rotational distributions[7]. The

aim of this paper is the study of those high vibrational levels previous to the closing of the above commented $\Delta v = -1$ exit channel, $v = 42, 43, 44$, which are suspected to exhibit to some extent IVR effects. vdW zero order states (ZOS) corresponding to different v manifolds presented in a previous work[6] to describe mixing effects found for $v = 45$-resonances are used again. Theoretical foundation for these states is similar to as vdW modes introduced by Halberstadt and collaborators [3] to explain IVR mechanism in $ArCl_2$ cluster. Limits of description in terms of these ZOS will be discussed in next sections.

In this work, the stabilization method is used to extract LS and resonance energies for $v = 42 - 45$. The method was initially proposed by Taylor *et al.* [15] for calculating energies and widths of resonances in electron-atom (or molecule) collisions and has been extensively used in a great variety of processes and systems, such as reactive scattering (see Refs. [16] to [32]) dissociative photoabsortion [33], and vdW complexes [6, 34, 35, 36, 37]. Concerning to the idea of stabilizing a root to obtain resonant energies, Taylor and collaborators [15, 17, 18] pointed out the close relationship between stabilization and some other techniques, as the scaling-variation orthogonalization procedure of Holöien [38] and the truncated diagonalization method of Lipsky and Russek [39]. The stabilization method uses $\mathcal{L}^2$ (or 'bound state' type) representations of continuum wave functions which, despite their approximative nature, provide an useful and quite accurate picture of quasi-bound states involved in scattering resonances. The key argument to justify the use of a square-integrable representation of continuum states is to consider the Hilbert space partitioned into P space (which refers to the asymptotic behavior of scattering functions) and Q space (the region of the space where resonance wave functions are thought to be localized)[15, 23]. It can be shown[15] that diagonalizing the Hamiltonian, H, in Q space is equivalent to diagonalize the pseudo Hamiltonian QHQ in the full Hilbert space, so basis sets with no inclusion of specific asymptotic scattering exit channels are adequate to calculate resonances.

The method basically consists on carrying out succesive diagonalizations of the Hamiltonian operator in slighty different basis sets which depend on a parameter (α). Differences among these sets correspond to variations on values of this so-called stabilization parameter. Those energy levels presenting a stable behavior with this parameter can be properly considered as bound states or resonances of the system under study. Other levels strongly depend of the stabilization parameter and do not present the quasi-vertical behavior of a proper resonance in a stabilization diagram, where the α parameter is plotted versus energy. In earlier works [15, 17, 18, 19, 20, 21, 22, 27] what was really varied was the size of the basis set and possible stable behavior of the energy levels was studied as the number of basis functions was increased.

At this point, it is interesting to mention the methods summarized by Thompson *et al.* [31] for the calculation of the resonance widths, depending on the kind of

information required from the stabilization calculation. Basically some of them [19, 35] use various versions of Fermi's GR as the formula proposed by Miller [40]. Fels *et al.* [20] used the fact that the slope of a stable root as a function of the basis size can be related to the resonance energy and width to extract both magnitudes. A procedure which involves only integrals of the stabilized function was employed by Taylor *et al.* [22]. Some other methods allow to obtain the width directly from the stabilization diagram [31, 36]. In particular, the formula obtained by Simons [36] only uses the resonant root and a non-resonant one with which exhibits an avoided crossing.

Succesive refinements of the original idea were made in order to obtain resonance parameters. Mandelshtam *et al.* [23] proposed an averaging procedure to calculate the density of states based on the idea of that P and Q contribute separately to this function. As long as the Q contribution can be fitted by a Lorentzian profile, parameters such as resonance positions and widths are straightforward to calculate. The same authors included in other work [33] the overlap between some convenient wave function and the stabilization one in the calculation of the density of states. This procedure was also used in the study of the $v = 45$ level of $HeBr_2$ by González–Lezana *et al.* [6]. A later contribution [34] consisted in a modification which enables to avoid the calculation of derivatives of the eigenvalues with respect to the stabilization parameter. Resonance parameters are extracted from a fit to the phase shift. More recently it has been suggested to substract the background phase in order to improve this last method [37].

In this paper, the underlying theory and basic equations of the stabilization method are given in Section 10.2. Results are presented and discussed in Section 10.3 and, finally, a brief conclusion is given in Section 10.4.

10.2 Theory

The cross section for the transition from a bound rovibrational level i of the ground (X) electronic state to a final f level in an excited (B) electronic state, within first order perturbation theory, is expressed as:

$$\sigma_i(E) \propto \omega \sum_f \mid \langle \Psi_{fE}(B) \mid \boldsymbol{\mu} \cdot \mathbf{e} \mid \Psi_i(X) \rangle \mid^2, \tag{10.1}$$

where ω and $\mathbf{e}$ are the frequency and polarization vector of the incident photon, respectively; $\boldsymbol{\mu}$ is the transition dipole moment for the $X \rightarrow B$ transition, while $\Psi_i(X)$ and $\Psi_{fE}(B)$ are bound and dissociative nuclear wave functions with energies E_i and

Table I. Parameters of the $HeBr_2(X,B)$ potential energy surfaces.

		$D(\mathrm{cm}^{-1})$	$\alpha(\mathring{A}^{-1})$	$\rho_e(\mathring{A})$
Br–Br	X	24557.674	1.588	2.281
	B	RKR	potential	(Ref.[41])
He–Br	X	19.62	1.55	3.81
	B	17.00	1.55	3.92

$E = E_i + \hbar\omega$, respectively. Both of them are eigenfunctions of total Hamiltonians of the form:

$$H^\epsilon = - \frac{\hbar^2}{2m}\frac{\partial^2}{\partial R^2} - \frac{\hbar^2}{2\mu}\frac{\partial^2}{\partial r^2} + \frac{\mathbf{l}^2}{2mR^2} + \frac{\mathbf{j}^2}{2\mu r^2} + V^\epsilon_{Br_2}(r) + W^\epsilon_{HeBr_2}(r,R,\theta) \tag{10.2}$$

expressed in Jacobi coordinates, where $\mathbf{r}$ is the vector joining the two Br nuclei, $\mathbf{R}$ is the vector going from the center of mass of Br_2 to the helium nucleus, and θ is the angle between $\mathbf{r}$ and $\mathbf{R}$. Reduced masses of Br_2 and $HeBr_2$ are written as μ and m, while $\mathbf{l}$ and $\mathbf{j}$ are angular momenta associated with vectors $\mathbf{R}$ and $\mathbf{r}$, respectively. Intramolecular and intermolecular interaction potentials are described by $V^\epsilon_{Br_2}$ and $W^\epsilon_{HeBr_2}$ for ground ($\epsilon = X$) and excited ($\epsilon = B$) electronic states. As in previous works[5, 6] both potential energy surfaces (PES) were constructed as a sum of pairwise Br-Br and He-Br interactions given by Morse functions, except for the B electronic state of Br_2 where an RKR potential extracted from spectroscopy data [41] was used. Parameters for the PES are shown in Table I.

The stabilization method uses a discrete representation of continuum wave functions. Square-integrable functions, $\mathcal{L}^2$- type, normally reserved to describe discrete states, are used to represent continuum states. In our study, they depend on a dimensionless parameter α, and are expanded in an analogous way as it is often used for the bound X-state[5, 6]. The dissociative wave function in the B state is thus written as

$$\Phi_m^{JMp_ip_j}(\boldsymbol{R},\, \boldsymbol{r};\alpha) \;=\; \sum_{vkj\Omega} b^m_{vkj\Omega}(\alpha)\; \varphi_k(R;\alpha)\; \chi_v(r)\; \Theta_{j\Omega}^{JMp_ip_j}(\hat{\mathbf{r}},\hat{\mathbf{R}}), \tag{10.3}$$

where $\chi_v(r)$ are eigenfunctions of the diatomic Hamiltonian $-(\hbar^2/2\mu)(\partial^2/\partial r^2) + V_{Br_2}(r)$, $\left\{\Theta_{j\Omega}^{JMp_ip_j}\right\}$ is a free rotor basis set[5, 42], with J as the total angular momentum, M and Ω its projections onto the space and body fixed z axes, respectively; p_i is the parity under inversion of nuclear coordinates, and p_j is the parity under bromine nuclei exchange. $\varphi_k(R;\alpha)$ functions contain the dependence of the basis on the stabilization parameter, α. They have been chosen to constitute an orthonormal basis set of discrete variable representation (DVR) functions, obtained from diagonalization of R-coordinate operator in an harmonic oscillator (HO) basis set, with a characteristic frequency depending on the α parameter:

$$\omega = \sqrt{\alpha}\;\; \omega_0, \tag{10.4}$$

ω_0 being a reference frequency. The DVR points for an HO set N functions are precisely the nodes of the $(N+1)$-th HO function. For a given value of α, $\Phi_m(\alpha)$ functions, defined in Eq.(10.3), and associated eiegenvalues $E_m(\alpha)$ are calculated by diagonalization of the Hamiltonian matrix. Variations of values of α affect the length of the R–coordinate space spanned by the DVR points. As the frequency ω increases, for instance, the DVR points will be localized in a shorter region, as the corresponding HO functions become more compact. So a proper range of values of the stabilization parameter must be considered. This range will contain those α's that generate spreaded enough DVR eigenvalues to describe discretized continuum wave functions of our molecular system and that guarantee an adequate density of points in the region of interest.

A discrete expression for the photofragmentation cross section is given by

$$\sigma_i(E;\alpha) \propto \sum_m \mid \langle \Phi_m(\alpha) \mid \boldsymbol{\mu}\cdot\mathbf{e} \mid \Psi_i(X)\rangle \mid^2\; \delta(E_m(\alpha) - E), \tag{10.5}$$

but analogously to Mandelshtam and coworkers' suggestions [23, 24, 25, 33], we define an average cross section by

$$\langle \sigma_i(E)\rangle \approx (\Delta\alpha)^{-1} \int_{\alpha_0}^{\alpha_0+\Delta\alpha} d\alpha\, \sigma_i(E;\alpha), \tag{10.6}$$

where α_0 and $\alpha_0 + \Delta\alpha$ limit the range of α's mentioned above.

Inserting Eq.(10.5) into Eq.(10.6), the average cross section is written as [23]:

$$\langle \sigma_i(E) \rangle \approx (\Delta\alpha)^{-1} \sum_m \left| \frac{dE_m}{d\alpha} \right|^{-1}_{\alpha^*_m} \langle \Phi_m(\alpha^*_m) \mid \mathcal{P}_{\mathcal{X}} \mid \Phi_m(\alpha^*_m) \rangle, \tag{10.7}$$

where $\mathcal{P}_X$ is the projector operator into X electronic state defined by

$$\mathcal{P}_X = \mid \boldsymbol{\mu} \cdot \mathbf{e} \Psi_i(X) \rangle \langle \boldsymbol{\mu} \cdot \mathbf{e} \Psi_i(X) \mid \tag{10.8}$$

and where the $E_m(\alpha)$ curve intersects the straight line $E = constant$. The calculation of photofragmentation cross sections from (10.7) for the most populated $X \rightarrow B$ vibronic transitions allows a realistic simulation of experimental excitation spectra. Such a simulation has been recently carried out by us using the close–coupling method [7]. In this work, however, we are rather interested in studying the resonance structure of the $HeBr_2(B, v = high)$ continuum. To this end, the stabilization calculations are carried out at $J = 0$ (with $p_j = +1$, $p_i = +1$) and, instead of computing the initial bound state $\Psi(X)$ and the effect of operator $\boldsymbol{\mu} \cdot \mathbf{e}$ in Eq.(10.7), we consider the operator

$$\mathcal{P}_{v_0} = \mid \chi_{v_0} \rangle \langle \chi_{v_0} \mid \tag{10.9}$$

that projects out the stabilization wave function onto a $v = v_0$ manifold:

$$\mathcal{P}_{v_0} \mid \Phi_m \rangle \; = \mid \Phi^{v_0}_m \rangle \; = \; \chi_{v_0}(r) \sum_{kj\Omega} b^m_{v_0 kj\Omega}(\alpha) \, \varphi_k(R;\alpha) \, \Theta^{JMp_ip_j}_{j\Omega}(\hat{\mathbf{r}}, \hat{\mathbf{R}}). \tag{10.10}$$

The total cross section can be finally written in a more compact way as

$$\langle \sigma_{v_0}(E) \rangle \approx (\Delta\alpha)^{-1} \sum_m \left| \frac{dE_m}{d\alpha} \right|^{-1}_{\alpha^*_m} w^{v_0}_m(\alpha^*_m) \tag{10.11}$$

where $w^{v_0}_m(\alpha^*_m)$ is the weight of the v_0 state within the total wave function:

$$w^{v_0}_m(\alpha) = \langle \Phi_m \mid \Phi^{v_0}_m \rangle = \sum_{kj\Omega} \mid b^m_{v_0 kj\Omega}(\alpha) \mid^2 . \tag{10.12}$$

Another goal of this work is the assignment of the resonance structures appearing in $\langle\sigma_{v_0}(E)\rangle$. To do so we define a set of ZOS

$$\Psi_n^v(\mathbf{r},\mathbf{R};\alpha) = \chi_v(r)\phi_{vn}(\mathbf{r},\mathbf{R};\alpha). \tag{10.13}$$

where ϕ_{vn} is an eigenstate of the projected Hamiltonian $H_v = \mathcal{P}_v H \mathcal{P}_v$. As the corresponding PES $W_v(r,R) = \langle\chi_v \mid W \mid \chi_v\rangle$ exhibits a well, ϕ_{vn} will correspond to bound states for the lower n-range whereas such wave functions will constitute "discretizations" of the continuum states for higher values of n. ZOS defined in Eq.(10.13) will be abreviately called (v,n) in the discussion below. Alternative cross sections can be obtained by defining the projection operator

$$\mathcal{P}_{v_0 n} = \mid \Psi_n^{v_0}\rangle\langle\Psi_n^{v_0} \mid, \tag{10.14}$$

therefore

$$\langle\sigma_n^{v_0}(E)\rangle \approx (\Delta\alpha)^{-1} \sum_m \left|\frac{dE_m}{d\alpha}\right|^{-1}_{\alpha_m^*} w_m^{v_0 n}(\alpha_m^*) \tag{10.15}$$

where $w_m^{v_0 n}(\alpha)$ is the weight of the ZOS within the total wave function and is written as,

$$w_m^{v_0 n}(\alpha) = \langle\Phi_m(\alpha) \mid \mathcal{P}_{v_0 n} \mid \Psi_n^{v_0}(\alpha)\rangle = \mid \langle\Phi_m(\alpha) \mid \Psi_n^{v_0}(\alpha)\rangle \mid^2 . \tag{10.16}$$

Finally, assuming that $\mid \Psi_{v_0 n}\rangle$ constitutes a complete basis within the $v = v_0$ manifold, it can be easily shown that

$$w_m^{v_0}(\alpha) = \sum_n w_m^{v_0 n}(\alpha). \tag{10.17}$$

Plotting eigenvalues $E_m(\alpha)$ (obtained by diagonalization at each given α), as functions of α provides the so–called stabilization diagram. Quasibound states can be distinguished from this diagram because of their stable behavior, *i.e.*, very pronounced slope $|dE_m/d\alpha|^{-1}$. So when non negligible overlaps are involved in the expression for the cross section, important peaks will appear when plotting $\langle\sigma(E)\rangle$. On the other hand, energies of continuum states present a higher variation with α–parameter.

The aim of using the stabilization method in this context is to obtain resonance parameters (energy positions and widths) and study the "intrinsic" structure (nodal patterns, overlaps with vdW ZOS, rotational and radial distributions[5, 6]) of the associated wave functions in those regions of the stabilization diagram where the most stable behavior is found. In addition, a qualitative description of cross section profiles can be achieved for the high vibrational levels under study.

In this work two types of calculations were conducted. First, zero order stabilization wave functions were obtained by diagonalizing the v–block Hamiltonian H_v using the same basis expansion as in the complete wave function from Eq.(10.3) but including just one vibrational function $\chi_v(r)$. Second, the full stabilization wave functions were computed including five vibrational levels $(v-3, v-2, v-1, v, v+1)$ in the expansion of Eq.(10.3).

In both calculations 12 rotational basis functions and 30 DVR functions for the vdW streching mode were included. The HO reference frequency was chosen to be the corresponding one to an harmonic approximation of the interaction potential at the T-shape configuration, *i.e.*, $\hbar\omega_0 = 22.45\, cm^{-1}$.

10.3 Results and discussion

10.3.1 Zero order states

Figs. 10.1 (a), (b) and (c) show the zero order stabilization diagrams for $v_0 = 43, 44, 45$ respectively. All energies are referred to the bottom of the B-electronic PES. In each panel, free diatomic vibrational energies are indicated with vertical dashed lines. First four $E_n(\alpha)$ curves, those below the diatomic levels mentioned above, represent (quasi)bound vdW states found for each vibrational state. Their energies referred to the Br_2 vibrational level are negative. The other eigenvalue–curves constitute discretized continuum states. It must be noted that the first ones still present a quasi–stable behavior (or at least not so unstable as the rest), as their energies do not undergo dramatic variations with the α–parameter. Fig. 10.1 also illustrates the fact that $(v_0, n \leq 3)$ levels are inmersed in the continuum of $(v < v_0, n > 3)$ ZOS. Interaction between these two kinds of states explains the existence of quasibound states (resonances).

The calculation of the ZOS also serves to define the optimal range of α values to be used in the full calculations. We have chosen this range to be between 0.08 and 1.10. Deviations from the expected stable behavior of $(v_0, n = 0)$ level for $\alpha > 1.10$ are attributed to the limit of validity of the DVR basis used here.

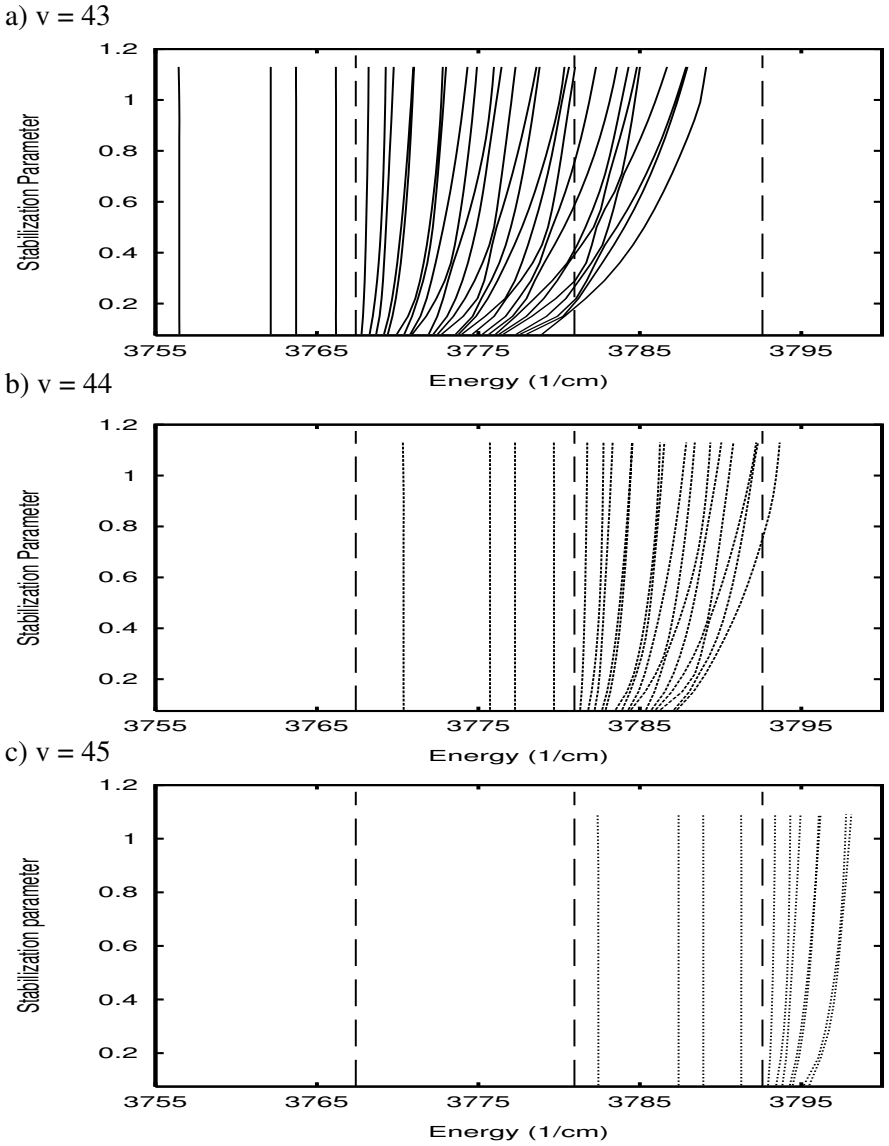

Figure 10.1: Zero order stabilization diagrams for (a) $v = 43$, (b) $v = 44$ and (c) $v = 45$ respectively. Energies, in cm^{-1}, are referred to the bottom of the B-electronic state. Diatomic vibrational energies for these vibrational states are marked with vertical dashed lines.

Table II. Energies (in cm^{-1}) of the bound zero order states $\Psi_n^{v_0}$, referred to the $Br_2(B, v_0)$ level.

n	$v_0 = 41$	$v_0 = 42$	$v_0 = 43$	$v_0 = 44$	$v_0 = 45$
0	-11.5001	-11.2394	-10.9350	-10.5800	-10.1587
1	-5.3480	-5.3090	-5.2715	-5.2280	-5.1861
2	-3.7350	-3.7181	-3.7030	-3.6777	-3.6561
3	-1.1490	-1.1891	-1.2310	-1.2600	-1.3016

In Table II, zero order energies for $42 \leq v_0 \leq 45$ are presented. They are measured with respect to the diatomic v_0 level. It should be noted that, due to the anharmonicity of the Br_2 vibration, (v_0, n)–states become closer to the diatomic level $v_0 - 1$ when increasing v. Thus, $(v_0 = 45, n = 0)$ is the closest state to the diatomic $(v_0 - 1)$–level with a value of $1.478\, cm^{-1}$.

We will show below that, despite of their approximative validity, these zero order calculations can bring some help in understanding the intrinsic dynamics of photodissociation from such high vibrational levels: LS for cross section profiles in a concrete vibrational level $v = v_0$ can be explained as the result of interaction among ZOS from v_0 and $v < v_0$.

10.3.2 Full calculations

In Fig. 10.2, the stabilization diagram for $v = 44$ is shown. Now, a completely stable behavior for the whole range of α at the energy of the resonances is not achieved any more. Interactions of the quasibound states with continua belonging to lower vibrational levels only allow small regions of the $E_n(\alpha)$ curve to behave in a more stable way. Positions of quasibound states can be extracted from these stabilization diagrams searching the stable regions, as the largest values for $|dE_m/d\alpha|^{-1}$ are associated to them (provided that overlaps considered in Eq.(10.11) are not too small). In particular from Fig. 10.2, two stable levels are found around -12.75 and -13.25 cm^{-1}. The region of the smallest values of α seems to be the most diffuse in order to notice a stable behavior of these levels.

Profiles obtained in the way described in the previous section(10.11) are shown in Fig. 10.3 (a), (b), (c) and (d) for v =42, 43, 44 and 45 respectively. In these figures, Br_2 vibrational levels are also indicated by vertical dashed lines. It is noticeable from the figure that whereas maxima for v =42 and 43 are located between v and $v - 1$ diatomic levels, the first peak for $v = 44$ is partially below the $Br_2(v = 43)$ level. For $v = 45$, this effect is even stronger as the first two peaks are totally inmersed below the $v = 44$ diatomic vibrational level. This feature is the closing of the $\Delta v = -1$ channel for the VP of $HeBr_2$. As it was first experimentally observed[10] and later theoretically reproduced by means of three dimensional quantum calculations [5], for vibrational excitations $v \geq 44$ of the cluster the vdW binding energy is larger than the difference between adjacent levels of the halogen fragment. Thus two vibrational quanta are required to break the bond between the He atom and the diatomic partner. For these levels a direct mechanism of fragmentation where the initial state, (B, v_0, n), directly couples to the $(v - 1)$ dissociative continuum is not longer possible and an indirect process where $(v_0 - 1, n \leq 3)$ states play the role of doorway states seems to be more adequate.

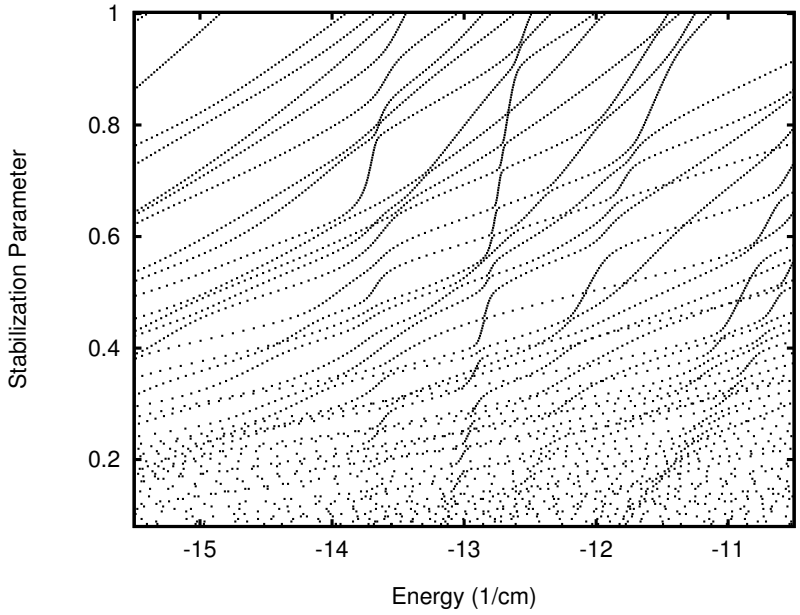

Figure 10.2: Stabilization diagram for $v = 44$. Energies are measured in cm^{-1} and are referred to Br_2–$(v = 44)$ level.

From Fig. 10.3 it can be noted that for each vibrational level, cross section peaks can be arranged in two groups: first group involves three (even four for $v = 45$) peaks clustered at energies just below the v diatomic levels, and a second group with one principal and two or three secondary maxima located at lower energies, closer to the corresponding $(v - 1)$-Br_2 levels. Disposition of these two groups keeps some resemblance with the structure observed for the bound ZOS in the previous zero order stabilization diagrams. This feature seems to suggest that the peaks can be assigned to the $(v_0, n \leq 3)$-ZOS. That conjeture is confirmed by calculating cross sections expressed in Eq.(10.15), that is, those which involve overlaps of wave functions obtained in every diagonalization with ZOS $(v = v_0, n)$ defined in Eq.(10.16).

In Fig. 10.4, the v_0–projected cross section for $v = 43$ is compared with the overlaps with the different ZOS $(v = 43, n = 0 - 3)$. The results confirm the direct association of resonance peaks with the ZOS. $\langle \sigma_{v_0} \rangle$ cross sections obtained from Eq.(10.11) is shown with solid line, whereas $\langle \sigma_n^{v_0} \rangle$ cross sections where n =0,1,2 and 3 are presented with diamonds, crosses, squares and $X-$shaped crosses respectively. Zero state energies are marked with vertical dashed lines. All energies, in cm^{-1}, are negative as they are referred to the $v_0 = 43$ vibrational level. In this figure, it can be noted the complete agreement achieved between the calculations performed with $\Psi_{n=0}^{v_0=43}$ and $\Phi_m^{v_0=43}$ in the region between -15.0 and $-10\ cm^{-1}$. It is also noticeable that calculations with every particular ZOS $\Psi_n^{v_0=43}$, where $n = 1, 2, 3$, perfectly determine positions of resonances found considering the projection within

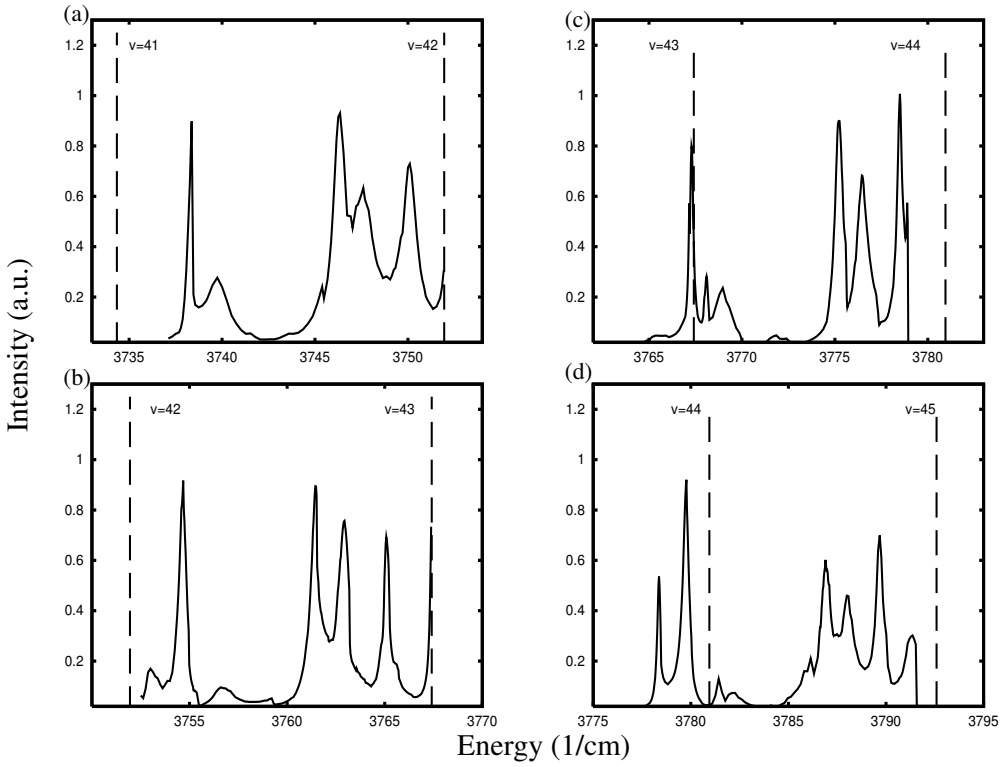

Figure 10.3: $\langle \sigma_{v_0}(E) \rangle$ cross section profiles from expression (10.7) for (a) $v_0 = 42$, (b) $v_0 = 43$, (c) $v_0 = 44$ and (d)$v_0 = 45$. Zero energy is defined as in Fig. 10.1 Arbitrary units were considered for intensities of the line shapes.

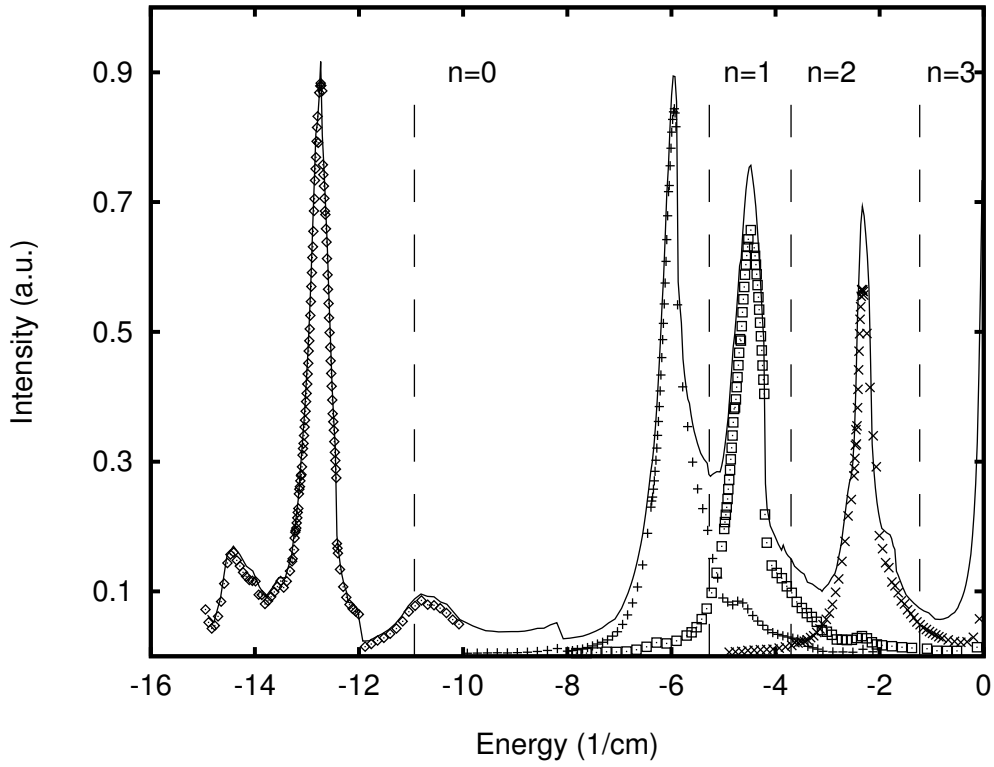

Figure 10.4: Comparison among $\langle \sigma_{v_0}(E) \rangle$ (solid line) and $\langle \sigma_n^{v_0}(E) \rangle$ cross section profiles with $v_0 = 43$ and $n = 0$ (diamonds), $n = 1$ (crosses), $n = 2$ (squares) and $n = 3$ ($X-$shaped crosses). Zero state energies are marked with vertical dashed lines. All the energies, in cm^{-1}, are negative as they are referred to the $v_0 = 43$ vibrational level.

Table III. Results obtained in full calculations for v_0 =42, 43, 44 and 45. First column indicates the n–label of the zero order associated to the peak. In cm^{-1}, the first entry of the column for each vibrational level corresponds to the energy of the resonance E (referred to the $Br_2(B, v)$ level), the second to the difference between the resonance and the zero order level, $\Delta_0 = E - E_0$, and the third shows the energy difference between the resonance and $Br_2(B, v-1)$ level, $\Delta_{v-1} = E - E_{v-1}$.

	v_0=42			v_0=43			v_0=44			v_0=45		
n	E	Δ_0	Δ_{v-1}	E	Δ_0	Δ_{v-1}	E	Δ_0	Δ_{v-1}	E	Δ_0	Δ_{v-1}
0	-13.60†	-2.36	4.02	-14.43	-3.49	1.03	-13.67†	-3.09	-0.13	-14.17	-4.01	-2.54
0	-12.18	-0.95	5.43	-12.76†	-1.82	2.70	-12.77	-2.18	0.77	-12.80†	-2.64	-1.17
0				-10.69	0.24	4.77	-11.86	-1.28	1.67			
1	-5.68	-0.37	11.93	-5.95	-0.68	9.51	-5.72	-0.49	7.82	-5.68	-0.50	5.95
2	-4.32	-0.60	13.30	-4.47	-0.77	10.98	-4.45	-0.77	9.08	-4.51	-0.85	7.13
3	-1.86	-0.67	15.75	-2.33	-1.10	13.13	-2.46	-1.20	11.08	-2.93	-1.63	10.33
3							-0.69	0.57	12.85	-1.33	-0.03	10.30

† Most intense peak.

the total vibrational state $v = 43$. Nevertheless contributions of these three excited n-states need to be considered in order to reproduce intensities of the peaks at intermediate regions among them. This interference effect seems to become stronger in the highest levels studied, $v = 44, 45$, where (v_0, n) states, with $n > 0$, were found to contribute even at the $(v_0, n+1)$–maximum position. Despite there are overlaps, the three peaks have Lorentzian shapes, and appear to be totally assigned by the $(v_0 = 43, n = 1, 2, 3)$ ZOS. The situation is different for the peaks of the lower energy region. The more complex shape of the cross section in this region suggests that there might be interactions with ZOS belonging to a different vibrational manifold (i.e. $v < v_0$). This issue is discussed in more detail below.

Results on resonance energies for all the vibrational levels studied in this work are listed in Table III. In this table, first column corresponds to the zero order level associated to each peak. Such an assignment was done through calculations performed to compute $\langle \sigma^{v_0}_{n\leq 3} \rangle$ cross sections defined in Eq.(10.15). The energies, E, of the different peaks found for each v, referred to Br_2 levels, are listed in the second column, while the third and the last columns correspond to the differences with the associated zero order levels, $\Delta_0 = E - E_0$, and with the $Br_2 - (v-1)$ level, $\Delta_{v-1} = E - E_{v-1}$ respectively. Notice that all maxima are red–shifted (*i.e.* shifted to lower energies), with respect to the ZOS positions. This feature confirms the limited validity of a zero order description of our problem; diagonalizations involving several vibrational levels are seriously needed in order to consider the existing interactions among them.

In Table III, the two more important peaks associated to the ground ZOS ($v_0, n =$

0) are indicated by L (left) and R (right). As it is pointed out at the table, one of these peaks is clearly more intense than the other. An interesting feature is the alternance between L and R resonances in being the most intense peak. Thus, whereas for $v = 42$ and $v = 44$ the L resonance is the most intense (see Figs. 10.3(a) and (c) respectively), for $v = 43$ and $v = 45$ the R resonance plays the role of the most intense of both (see Figs. 10.3(b) and (d) respectively).

In order to study more carefully the R and L resonances, adequate values of α were chosen from stabilization diagrams for $v = 42, 43, 44$ and 45 and overlaps $w_m^{vn}(\alpha_m)$ defined by Eq.(10.16) with $v \leq v_0$ and $n \leq 50$ were calculated. This decomposition in ZOS is shown in Fig. 10.5. Weights corresponding to different v levels are shown in various shades and are labelled at the figure.

As can be seen from Fig. 10.5, the most intense peak always corresponds to the resonance with the highest component on the $(v_0, n = 0)$ state, being this ZOS the one receiving the major overlap in all the cases studied, whereas for the secondary maximum a higher presence of $(v_0 - 1, n)$ states is found. All levels show a strong mixing among (at least) v and $v - 1$ levels for the most intense peak; thus, in particular for $v = 42$ and 44 (for which this peak corresponds to the R resonance) although the ZOS with the highest overlap is $(v_0, n = 0)$ in both cases, the total component on $v = v_0 - 1$, $w_m^{v_0-1}$, is about 55 % while $w_m^{v_0}$ is approximately 35 %. For $v = 43$ and 45 (for which L resonance is the most intense peak) the situation is a bit different in the sense that although $w_m^{v_0}$ is the highest in both levels (about 48 % and 32 % respectively) $v_0 - 2$ level takes part in the mixing with similar values as $w_m^{v_0-1}$. More precisely, $w_m^{v_0-1} = 22\%$ and $w_m^{v_0-2} = 21\%$ for $v_0 = 43$ and $w_m^{v_0-1} = 28\%$ and $w_m^{v_0-2} = 31\%$ for $v_0 = 45$. For the less intense peaks, ZOS from the $v_0 - 1$ level always present the highest overlaps and for all the v_0 studied $w_m^{v_0-1}$ is greater than the component from any other vibrational level. $w_m^{v_0}$ takes values about a 10 % (always accounted for the $(v_0, n = 0)$ state) in all cases.

On the other hand, it can be noticed that, the higher the level v, the lower the n levels of the $v_0 - 1$ manifolds showing important contributions to the resonances. This constitutes an expected result in view of the anharmonicity of the Br_2 vibration (see also Δ_{v-1} values in Table III). In other words, $(v_0, n = 0)$ faces lower $(v_0 - 1, n)$ states when increasing v's are considered. Thus, while the most important ZOS in the decomposition of the most intense peak is $n = 10$ for $v_0 = 42$, for $v_0 = 43$ is $n = 6$, and $n = 4$ for $v_0 = 44$. $v_0 = 45$ is the first level for which a discrete ZOS, $n \leq 3$, of the $v_0 - 1$ level is found to be facing the corresponding $(v_0, n = 0)$ state. The same set of $(v_0 - 1, n)$ states are the ZOS contributing to the secondary peak. In summary, it appears that for $v \leq 44$ levels, for which the $\Delta v = -1$ channel is still open, an IVR mechanism is also important, where the "bright" state $(v, n = 0)$ couples with one or more "quasibound" states $(v - 1, n > 3)$ (intermediate states) before coupling with continuum states causes the molecular fragmentation. The nature of these quasibound states (whether they can be understood of shape of

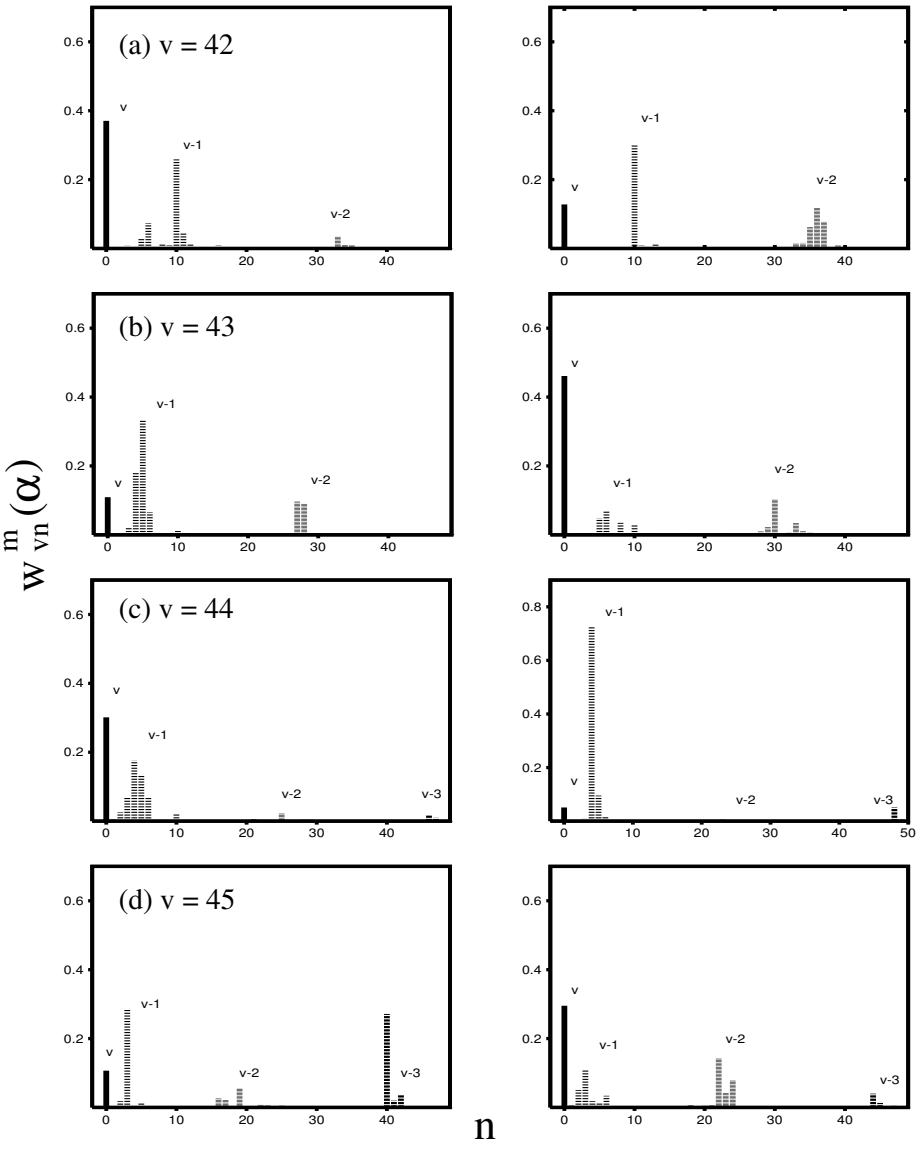

Figure 10.5: Weights $w_m^{v_0 n}$, defined by Eq.(10.16), as function of n, of the ZOS (v_0, n),$(v_0 - 1, n)$,$(v_0 - 2, n)$ and $(v_0 - 3, n)$ on the L and R resonances associated to $(v_0, n = 0)$. The values for $\alpha_m^{(L,R)}$ and associated energies $E_m^{(L,R)}$ corresponding to the stabilization wave functions Φ_m chosen for this decomposition are the following: (a) corresponds to $v = 42$ with $\alpha_m^{(L)} = 0.9000$ and $E_m^{(L)} = -13.54\, cm^{-1}$, and $\alpha_m^{(R)} = 0.8325$ and $E_m^{(R)} = -12.09\, cm^{-1}$, (b) is for $v = 43$ $\alpha_m^{(L)} = 0.8000$ and $E_m^{(L)} = -14.35\, cm^{-1}$, and $\alpha_m^{(R)} = 0.7010$ and $E_m^{(R)} = -12.89\, cm^{-1}$, (c) is for $v = 44$ $\alpha_m^{(L)} = 0.7550$ and $E_m^{(L)} = -13.63\, cm^{-1}$, and $\alpha_m^{(R)} = 0.7550$ and $E_m^{(R)} = -12.70\, cm^{-1}$ and finally (d) is for $v = 45$ $\alpha_m^{(L)} = 0.4715$ and $E_m^{(L)} = -14.28\, cm^{-1}$, $\alpha_m^{(R)} = 0.4265$ and $E_m^{(R)} = -12.82\, cm^{-1}$. At each panel, overlaps on $\Psi_n^v(\alpha)$ functions corresponding to different v levels are separately labelled.

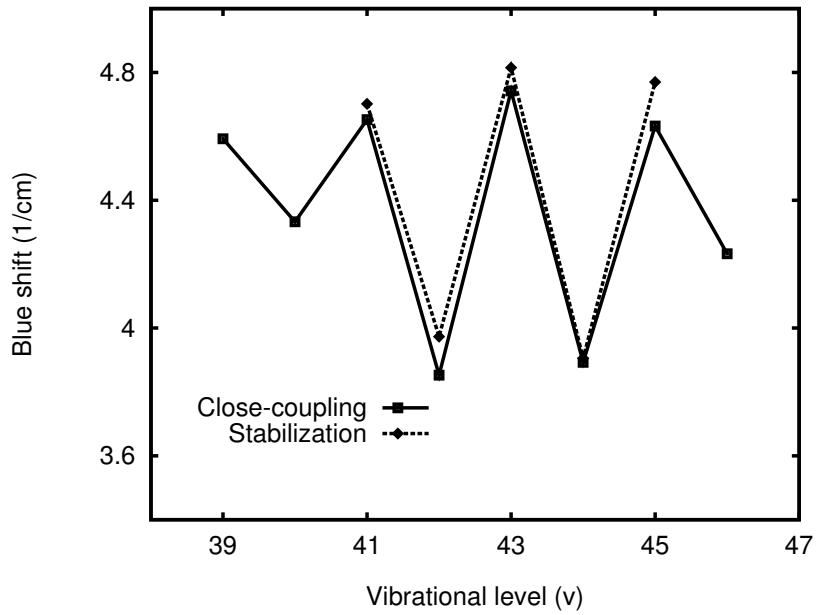

Figure 10.6: Spectral shifts $E_v(B) - E_i(X)$ (in cm^{-1}). Comparison between results from close–coupling (solid line and squares) and stabilization calculations (dashed line and diamonds) is presented.

orbiting resonances, for instance) could be the subject of a future investigation.

The origin of the remaining peak associated to $n = 0$ but with lower intensity than those of the R and L peaks could be explained from the following considerations: they are located close to $(v_0, n = 0)$–zero order positions (so the overlap with that state must not be negligible) and are crossed by some $(v_0 - 1, n)$ states, with n not too high (so $|dE_m/d\alpha|^{-1}$ values are still large enough not to neglect them). This interpretation explains as well the absence of secondary and 'residual' minima associated to $(v_0, n = 0)$ resonances in lower vibrational levels: energy differences with the $(v_0 - 1)$–diatomic level are much larger and $(v < v_0, n)$–discretized continua crossing the $(v_0, n = 0)$ resonance region usually are much more unstable.

In a previous work [6], the stabilization $(v_0 = 45, n = 0)$ cross section profiles were compared with close–coupling calculations: agreement describing the two main peaks was achieved while the interaction region between them is better described by the close–coupling procedure. For $v < 45$, however, intrinsic difficulties involving an accurate description of the continuum states near threshold of the $v - 1$ channel made a satisfactory comparison with the close–coupling LS much harder. This problem disappears for v's further from the closing of the one quantum channel $(v < 40)$. Nevertheless, the stabilization method continues to be a powerful tool in determining resonance energies. In Fig. 10.6 spectral shifts $E_v(B) - E_i(X)$, measured in cm^{-1}, derived from stabilization (dashed lines and diamonds) and close–coupling

calculations (solid lines and squares) are compared. The figure includes the result for $v = 41$ although a more detailed study of that level has not been presented in this work. As it was explained before [5], $E_v(B)$ and $E_i(X)$ are vdW energies considered respect to the He+$Br_2(B, v)$ and He+$Br_2(X, v = 0)$ dissociation limits. The ground state energy for X–electronic state was $E_i(X, v = 0) = -17.573\, cm^{-1}$. Agreement with previous close–coupling calculations from the reference [5] is extremely good as the oscillatory behavior of the blue shifts found there is perfectly described.

10.4 Concluding remarks

Stabilization calculations have been carried out to study the VP of the $HeBr_2$ molecule for highly excited vibrational levels ($42 \leq v \leq 45$). The method offers an extremely appreciable help to study the intrinsic dynamics of the complex coming from such high levels. A zero order description facilitates the understanding of the cross section profiles obtained in each level. Assignment of peaks found for a given level to (v, n)-discrete vdW states was possible within this method. A typical double–peaked structure associated to $(v, n = 0)$ was explained by means of the stability of ZOS of the $v - 1$ manifold. It is concluded that the most intense peak always arises from a strong interaction between v_0 and $v_0 - 1$ levels ($v_0 - 2$ also contributes when the R resonance is the most intense peak), while the secondary peak is basically assigned to the $v_0 - 1$. In this way, we have found that an indirect mechanism of dissociation, where resonances of the $v - 1$ manifold play the role of intermediate states, is important for these high levels. So for lower vibrational levels,$v < 40$, absence of a double–peaked pattern is an expected result in light of the present analysis, as the corresponding states $(v < v_0, n)$ are highly unstable and have not a considerable contribution to the cross section profile.

The closing of the $\Delta v = -1$ channel is perfectly reproduced by the stabilization method. As a matter of fact, $v = 45$ is the first level where the interaction between ZOS might be properly called 'discrete–discrete', as $(v_0 = 45, n = 0)$ and $(v_0 = 44, n = 3)$ are the states involved.

Comparison of spectral shifts deduced from stabilization results with some previous close–coupling calculations[5] confirms the strength of the method in order to determinate resonance positions.

10.5 Acknowledgements

This work has been partially supported by the DGICYT Grant PB95-0071 (Spain), the European TMR Network ERBFMRX-CT96-0088 and the Spanish-Cuban Project between CSIC and Agencia the Ciencia y Tecnologia Cubana.

Bibliography

[1] S. K. Gray and O. Roncero, J. Phys. Chem. **99**, 2512 (1995); O. Roncero and S. K. Gray, J. Chem. Phys. **104**, 4999 (1996).

[2] D. D. Evard, C. R. Bieler, J. I. Cline, N. Sivakumar, and K. C. Janda, J. Chem. Phys. **89**, 2829 (1988).

[3] N. Halberstadt, J. A. Beswick, O. Roncero, K. C. Janda, J. Chem. Phys. **96**, 2404 (1992); N. Halberstadt, S. Serna, O. Roncero, K. C. Janda, J. Chem. Phys. **97**, 341 (1992); O. Roncero, P. Villarreal, G. Delgado–Barrio, N. Halberstadt, K. C. Janda, J. Chem. Phys. **99**, 1035 (1993); K. C. Janda, O. Roncero and N. Halberstadt, J. Chem. Phys. **105**, 5830 (1996); O. Roncero, D. Caloto, K. C. Janda and N. Halberstadt, J. Chem. Phys. **107**, 1406, (1997).

[4] O. Roncero, J. Campos-Martínez, A. M. Cortina, P. Villarreal and G. Delgado–Barrio, Chem. Phys. Lett. **148**, 62 (1988).

[5] T. González–Lezana, M. I. Hernández, G. Delgado–Barrio, A. A. Buchachenko and P. Villarreal, J. Chem. Phys. **105**, 7454 (1996).

[6] T. González–Lezana, M. I. Hernández, G. Delgado–Barrio and P. Villarreal, J. Chem. Phys. **106**, 3216 (1997).

[7] A. Rohrbacher, T. Ruchti, K. Janda, A. A. Buchachenko, M. I. Hernández, T. González–Lezana, P. Villarreal and G. Delgado–Barrio, J. Chem. Phys. **110**, 256 (1999).

[8] L. J. van de Burgt, J. P. Nicolai, M. C. Heaven, J. Chem. Phys. **81**, 5514 (1984).

[9] N. Sivakumar, J. I. Cline, C. R. Bieler, K. C. Janda, Chem. Phys. Lett. **147**, 561 (1988).

[10] D. G. Jahn, S. G. Clement, K. C. Janda, J. Chem. Phys. **101**, 283 (1994).

[11] D. G. Jahn, W. S. Barney, J. Cabalo, S. G. Clement, A. Rohrbacher, T. J. Slotterback, J. Williams, K. C. Janda and N. Halberstadt, J. Chem. Phys. **104**, 3501 (1996).

[12] T. González–Lezana, M. I. Hernández, G. Delgado–Barrio and P. Villarreal, J. Molec. Struc. (Theochem) **433** 107 (1998).

[13] P. J. Krause and D. C. Clary, Chem. Phys. Lett. **271**, 171 (1997).

[14] J. A. Beswick and J. Jortner, Adv. Chem. Phys. **47**, 363 (1981).

[15] H. S. Taylor, G.V. Nazaroff and A.Golebieswki, J. Chem. Phys. **45**, 2872 (1966).

[16] I. Eliezer, H. S. Taylor and J. K. Williams, J. Chem. Phys. **47**, 2165 (1967).

[17] H. S. Taylor, Adv. in Chem. Phys. **18**, 91 (1970).

[18] A. U. Hazi and H. S. Taylor, Phys. Rev. A J. Chem. Phys. **1**, 1109 (1970).

[19] M. F. Fels and A. U. Hazi, Phys. Rev. A **4**, 662 (1971); Chem. Phys. Lett. **8**, 582 (1971)

[20] M. F. Fels and A. U. Hazi, Phys. Rev. A **5**, 1236 (1972).

[21] H. S. Taylor and L. D. Thomas, Phys. Rev. Lett. **28**, 1091 (1972).

[22] H. S. Taylor and A. U. Hazi, Phys. Rev. A **14**, 2071 (1976).

[23] V. A. Mandelshtam, T. R. Ravuri, and H. S. Taylor, Phys. Rev. Lett. **70**, 1932 (1993).

[24] V. A. Mandelshtam and H. S. Taylor, J. Chem. Phys. **99**, 222 (1993).

[25] V. A. Mandelshtam, T. R. Ravuri, and H. S. Taylor, J. Chem. Phys. **101**, 8792 (1994).

[26] V. A. Mandelshtam, H. S. Taylor, C. Jung, H. F. Bowen and D. J. Kouri, J. Chem. Phys. **102**, 7988 (1995).

[27] T. C. Thompson and D. G. Thrular, J. Chem. Phys. **76**, 1790, (1982).

[28] T. C. Thompson and D. G. Thrular, Chem. Phys. Lett. **101**, 235 (1983); T. C. Thompson and D. G. Thrular, J. Phys. Chem. **88**, 210 (1984); J. G. Lauderdale and D. G. Thrular, J. Chem. Phys. **84**, 192 (1986).

[29] M. I. Hernández and D. C. Clary, J. Chem. Phys. **101**, 2779 (1994).

[30] T. González–Lezana and D. E. Manolopoulos, Farad. Discuss. **110**, 213 (1998).

[31] T. C. Thompson and D. G. Thrular, Chem. Phys. Lett. **92**, 71 (1982).

[32] B. Gazdy and J. M. Bowman, Adv. in Mol. Vib. and Coll. Dyn., **1B**, 105 (1991).

[33] V. A. Mandelshtam, T. R. Ravuri, and H. S. Taylor, Phys. Rev. **A48**, 818 (1993).

[34] V. Ryaboy, N. Moiseyev, V. A. Mandelshtam, and H. S. Taylor, J. Chem. Phys. **101**, 5677 (1994).

[35] Z. Bačlć and J. Simons, J. Phys. Chem. **86**, 1192 (1982).

[36] J. Simons, J. Chem. Phys. **75**, 2465 (1981).

[37] R. F. Salzgeber, U. Manthe, Th. Weiis and Ch. Schlier, Chem. Phys. Lett. **249** 237 (1995).

[38] E. Holöien and J. Midtdal, J. Chem. Phys. **45**, 2209, (1966) (*and earlier works referenced therein*).

[39] L. Lipsky and A. Russek, Phys. Rev. **142**, 59 (1966).

[40] W. H. Miller, Chem. Phys. Lett. **4**, 627 (1970).

[41] R. F. Barrow, T. C. Clark, J. A. Coxon, and K. K. Yee, J. Mol. Spectroscopy **51**, 428 (1974).

[42] O. Roncero, J. A. Beswick, N. Halberstadt, P. Villarreal, G. Delgado–Barrio, J. Chem. Phys. **92**, 3348 (1990).